Thermoplastic elastomers

R. Bonart
Institute of Applied Physics, University of Regensburg, W. Germany
(Received 8 July 1979)

Thermoplastic elastomers are crosslinked by secondary valence interactions. They show rubber elasticity at service temperatures but may be thermoplastically processed at elevated temperatures, i.e. they may be injection-moulded or, in special cases, spun from solution. Secondary valence interactions give rise to a continuous crosslink spectrum controlling the segment mobility in its low temperature region but controlling the crosslinking stability in its high temperature region. Crosslinking, which partly breaks down on heating the sample, is restored when the sample is cooled. Consequently, a stress crosslinking may be distinguished from strain crosslinking which is formed on cooling the deformed material, thus stabilizing the deformation. Stress and strain crosslinking systems reflecting the thermomechanical history are seen from shrinkage experiments.

INTRODUCTION

Conventional rubbers are crosslinked by primary valence bonding, whereas thermoplastic elastomers are crosslinked by secondary valence bonding, such as van der Waals interactions, dipole interactions or hydrogen bonding. The secondary valence crosslinking breaks down at an elevated temperature or under the influence of suitable solvents and will reappear with decreasing temperature or after the solvent has been removed. In principle, no damage to the material results from the breakdown and restoration of crosslinking. Consequently, while some thermoplastic elastomers are processable by injection-moulding, others can be spun from solution.

Thermoplastic elastomers show two transition temperatures, a lower one corresponding to the freezing-in or appearance of segment mobility and an upper one corresponding to the breakdown or restoration of secondary valence crosslinking. Freezing or softening takes place within two temperature regions which may be partly superimposed; sometimes it is hardly possible to observe a clear distinction between them. Since in both cases only secondary interactions are involved, uniform softening processes have to be considered. These processes may be described by a temperature- and time-dependent formal number of crosslinks per unit volume, $N(T,t)$, equal to the number of crosslinks in a Gaussian network which would show the same modulus of elasticity as the material under investigation. This formal number $N(T,t)$ is called the crosslink spectrum for the thermoplastic elastomer. It refers simultaneously to the crosslinking stability in a strict sense and to the segment mobility. With increasing temperature, $N(T,t)$ drops in two more-or-less pronounced steps corresponding to segment mobility setting in and crosslinking breaking down. Both steps have to be considered as part of one-and-the-same crosslink spectrum, since in many cases they are not clearly separated from each other.

The crosslink spectrum $N(T,t)$ may be modelled in a purely phenomenological way by the two sets of Maxwell elements in *Figure 1*, one of them characterizing the segment mobility and the other the thermal crosslink stability. Maxwell systems are well known from linear viscoelastic analysis of polymers where they are used to represent the relaxation time spectrum. With respect to thermoplastic elastomers, however, they are useful for describing the crosslink spectrum. In this case freezing or softening temperatures are of interest. The crosslink spectrum indicates the temperature ranges within which certain parts of the overall crosslinking breakdown or reappear. Each element of the Maxwell system represents a partial crosslinking which is characterized by a distinct freezing or softening temperature.

Thermoplastic elastomers may be distinguished both in a broad sense and in a technical sense, as follows. In a broad sense, all chemically uncrosslinked polymers can behave as thermoplastic elastomers. Starting from the glassy state, amorphous thermoplastics show rubber elasticity and then pure viscous flow with increasing temperature. The crosslinking is brought about by secondary valence interactions and chain entanglements. In partly crystalline thermoplastics crosslinking is also due to crystalline regions. In addition to

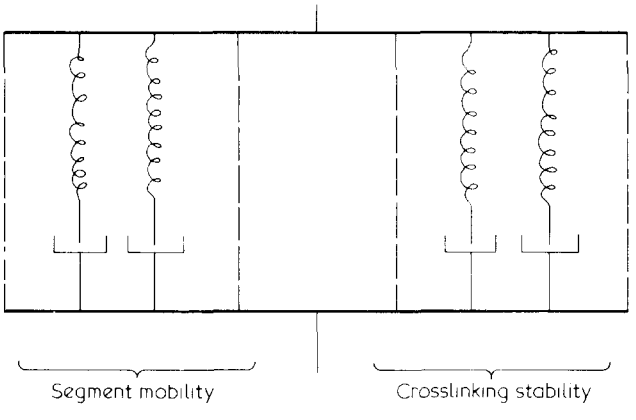

Figure 1 Maxwell representation of the crosslink spectrum of thermoplastic elastomers. Elements which are more unstable are responsible for the segment mobility, while more stable elements are responsible for the crosslinking stability. Additional elements in between the two sets may influence the stress-strain behaviour.

0032–3861/79/111389–15$02.00

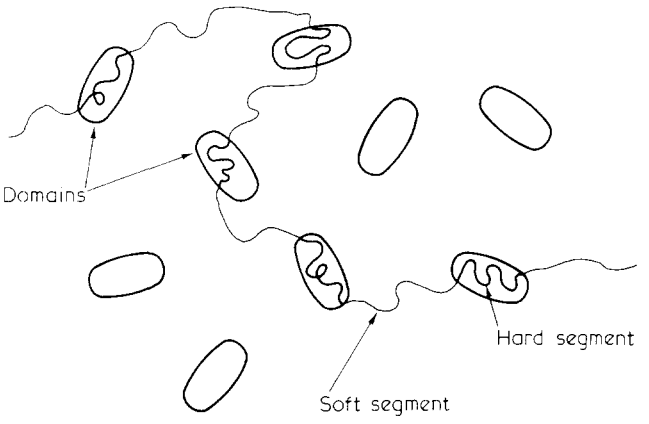

Figure 2 Secondary valence crosslinking due to domain formation with segmented chains

the rubber elasticity of amorphous thermoplastics, frozen-in elasticity and shrinkage have to be considered as typical characteristics of thermoplastic elastomers; these occur in amorphous and partly crystalline materials, as well as in technical thermoplastic elastomers.

Thermoplastic elastomers are segmented copolymers with hard and soft segments. A domain structure forms on segregation, characterized by hard segment domains dispersed in a soft segment matrix (*Figure 2*). At service temperatures, the domains are either crystalline or glassy, where the matrix is in a molten state. Since the molecules consist of alternating hard and soft segments, each chain runs alternately through the domains and the matrix. Thus, the domains are linked by main valence chains. The matrix in its molten state provides high extensibility, and the rigid hard segment domains prevent viscous flow, with the result that rubber elasticity is brought about. The chains linking the domains are crosslinked due to secondary valence bonding within the domains. Crosslinking breaks down as soon as the glassy transition temperature or the melting temperature of the domains is exceeded. Examples of important engineering thermoplastic elastomers are: segmented styrene–butadienes, ether–ester elastomers and segmented polyurethanes.

The dissociation energy of secondary valence interactions is smaller than that of main valence bonds by one or two orders of magnitude. However, since the secondary interactions are effective simultaneously and cooperatively within the domains, they provide a crosslinking with high thermal and mechanical stability, comparable with the stability of conventional corsslinking by main valence bonding.

The crosslink spectrum is closely correlated to the viscoelastic properties of the hard and soft segments and the degree of segregation. Let us assume that the softening (glass transition or melting) of two hompolymers A and B occurs at T_A and T_B, respectively (*Figure 3*). The softening temperature of a statistical A–B copolymer is found between T_A and T_B, closer to either the first or the second depending on the ratio A:B in the copolymer. Segmented block copolymers show simultaneously two different softening temperatures near T_A and T_B, respectively. Depending on the ratio A:B, an A matrix with B domains results or *vice versa*. The first is true for thermoplastic elastomers, the latter for high impact thermoplastics. Non-statistical copolymers with only short blocks give rise to a disproportion of local A and B concentrations without phase separation occurring. Hence different volume elements show different softening temperatures spread widely over the whole range from T_A to T_B. The disproportion of local concentrations rises with increasing block length, finally resulting in phase separation including disordered segments. Disordered B units dispersed in the A matrix will raise the softening temperature from T_A to $T_{A'}$. Disordered A units running through the B domains will lower the softening temperature from T_B to $T_{B'}$. Since disordered segments may be non-uniformly distributed, forming small aggregates, a certain effect of disproportion will remain, giving rise to an overlap of the softening regions at $T_{A'}$ and $T_{B'}$. Furthermore the existence of poorly defined domain boundaries results in a similar effect and has also to be taken into account. When discussing the crosslink spectrum it is useful, therefore, to investigate the domain structure at the same time, since the crosslink spectrum depends very much on the segregation of hard and soft segments.

The hard segment domains act as crosslinking volumes with high functionality. Since they have diameters of 100 Å or more, they are not comparable with conventional Gaussian network points and they act simultaneously as a filler, thus raising the elastic modulus. However, in contrast with fillers in conventional rubbers they do not reduce the breaking strain, since being in a material under macroscopic load, they will be partly deformed. This reduces local stress and improves the homogeneity of the stress field within the material, resulting in an increase in the breaking strength and strain. However, since the domains undergo plastic deformation, the retractive force will decrease (*Figure 4*). This causes a stress–strain hysteresis and a so-called permanent set, which is actually a frozen-in deformation of the material and will vanish when the material is heated.

The molecular deformation process is entirely different from that which is known about Gaussian networks. It is impossible, therefore, to define a crosslinking density rigo-

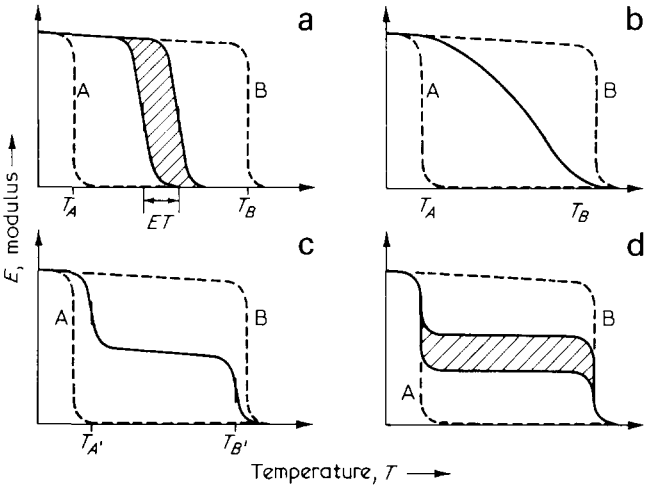

Figure 3 Schematic draft of the temperature dependence of Young's modulus for copolymers. The curves A and B show the softening behaviour of the pure components, respectively. Statistical A–B copolymers: (a) become soft in a distinct temperature between A and B, closer to A or to B dependent on the ratio of A to B. The softening of non-statistical copolymers with only short blocks; (b) not giving rise to phase separation is widely spread over the whole range from T_A to T_B. Segmented block copolymers (c) with imperfect phase separation show two distinct softening temperatures $T_{A'}$ and $T_{B'}$ which may differ from T_A and T_B because of misordered segments and unsharp domain boundaries. Segmented block copolymers showing perfect phase separation give rise to partial softening exactly at T_A and T_B, the modulus in between being dependent on the ratio A to B

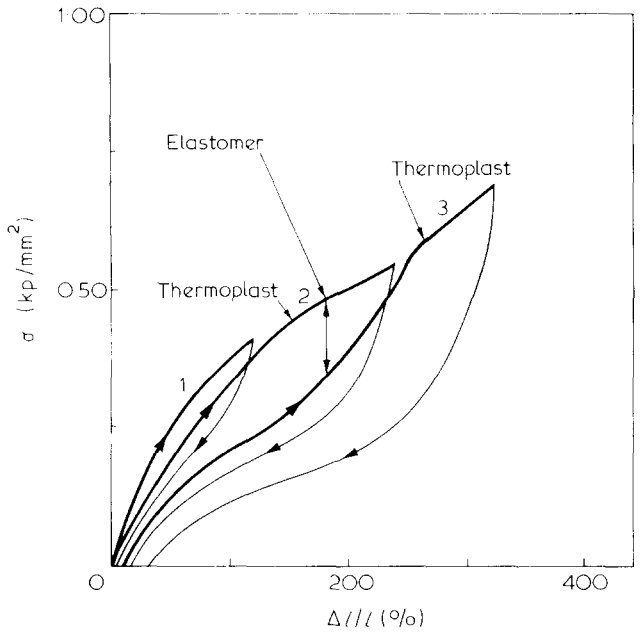

Figure 4 Typical stress–strain behaviour of segmented polyurethanes

rously in terms of the number of crosslinks per unit volume, since there are no distinct single crosslinks, but multifunctional crosslinking volumes which undergo plastic deformation. The *formal* number of crosslinks, therefore, merely is a formal number without any structural meaning, but which may be used in comparing different states of a material as well as different materials. The formal number of crosslinks i.e. the crosslink spectrum, of a given material depends on temperature and time and furthermore on load, strain and thermomechanical prehistory. The evaluation of this very complex spectrum is a major problem in the understanding of thermoplastic elastomers. Some special aspects of the crosslink spectrum will be presented in this paper.

SEGMENTED BLOCK COPOLYMERS

Segmented polystyrene -butadienes are prepared by anionic polymerization. Two-, three- and multiblock chains may be obtained with segments of statistical or well-defined length up to several hundred Ångstroms. Segment segregation is seen from electron micrographs after staining the polybutadiene sequences with osmium tetroxide. Model two- and three-block chains with segments of well-defined length give rise to highly periodic morphologies. With increasing amounts of styrene, starting at a low level, the styrene sequences form globular, rod-like and finally lamellar domains. At a hard segment content of more than 50%, lamellae grow together to form a matrix with rod-like and finally with globular polybutadiene inclusions. Chains with more than three segments each or with segments of statistically varying length do not segregate, but form irregular morphologies. Technical products are characterized by sponge-like arrangements of hard and soft segment regions (*Figure 5*).

Segmented polyether–ester elastomers prepared by transesterification of poly(tetramethylene oxide) with poly(tetramethylene terephthalate) show randomly jointed ester and ether segments, the statistically varying degrees of polymerization of which are m and n, respectively:

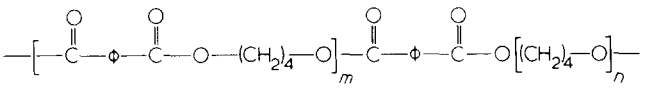

At room temperature, polyester crystallites are found creating hard segment domains, whereas the ether segments remain in the molten state. Spherulitic structures exist under certain conditions due to characteristic mutual arrangements of hard segment polyester crystallites within the molten polyether matrix.

Segmented polyurethanes are prepared *inter alia* from diphenylmethane diisocyanate (MDI):

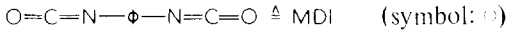

with ether-based or ester-based macrodiol, (symbol: ~)

the molecular weight of which lies in the region of approximately 1500 to 3000. Diols or diamines, such as, for example:

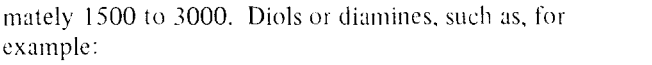

are effective as chain extenders.

In the prepolymer procedure diisocyanate and macrodiol are brought to reaction-forming urethane groups by addition:

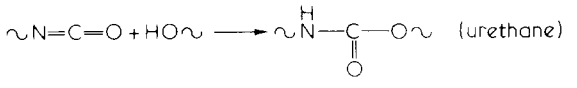

Applying more than 2 mol of diisocyanate (MDI) per mol of macrodiol results in a statistical distribution of prepolymer molecules with an additional amount of unreacted excess MDI. The prepolymer configurations may be described by:

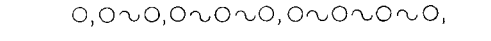

The prepolymer molecules are linked together by adding a suitable amount of chain extender, giving rise to urethane or urea coupling, respectively, dependent on whether a diol or a diamine extender is used. The urea coupling is defined by:

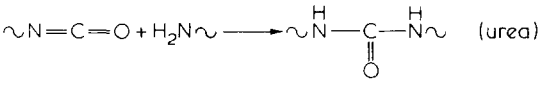

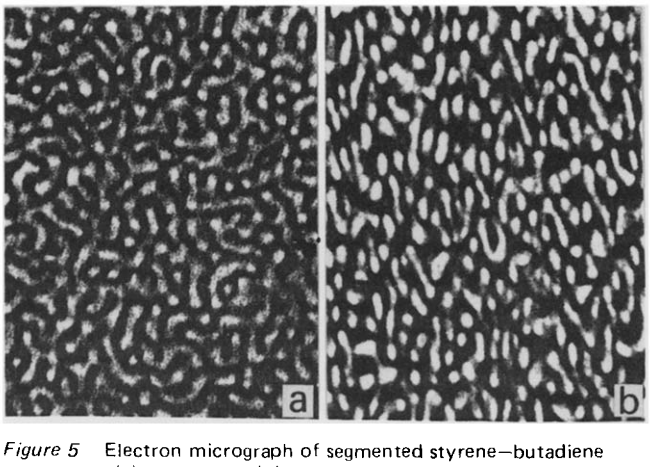

Figure 5 Electron micrograph of segmented styrene–butadiene elastomers: (a) unstrained, (b) after being strained and relaxed

Thus, essentially linear chains are obtained providing a statistical configuration composed of hard and soft segments:

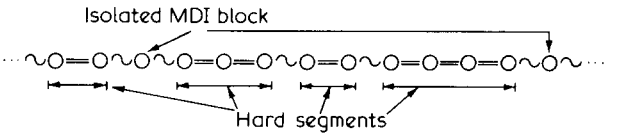

Hard segments are brought about by alternating sequences of diisocyanate and chain extender. Soft segments are virtually identical with the macrodiol, except for isolated diisocyanate blocks joined directly to macrodiol on both sides. These isolated blocks contribute both to the hard segments as well as to the soft segments in a manner which is dependent on the state of segregation.

The hard segment length follows a statistical distribution which corresponds under certain generally realized conditions to the molecular weight distribution of the condensation products. The distribution is controlled by the amount of unreacted excess MDI in the prepolymer, being detectable by means of gel permeation chromatography. It is controlled, therefore, by the molar ratio w of macrodiol to MDI. The percentage of hard segments with p MDI blocks each dependent on w is given by:

$$\psi_p = (1-w)^{p-1}w \tag{1}$$

resulting in a mean value

$$p = \sum_{p=1}^{\infty} p\psi_p = \frac{1}{w} \tag{2}$$

if isolated MDI blocks (defined by ~O~) are also taken into account. Neglecting isolated MDI blocks, i.e. considering them as part of the soft segments, leads to a mean value:

$$\bar{p}' = 1 + \frac{1}{w} \tag{3}$$

In segmented polyurethanes the statistical length distribution of the hard segments gives rise to diffuse domain boundaries since no chain-folding of the hard segments occurs. Segregated hard segments are virtually fully extended, and thus penetrate the matrix depending on their length. This is not the case in either segmented styrene–butadiene elastomers or segmented polyether–esters, where sharp domain boundaries occur, due to hard segment chain-folding. Soft segment conformations differ correspondingly in the vicinity of the domain boundaries, as shown schematically in *Figure 6*. Soft and hard segments are packed laterally in a similar manner in segmented polyurethanes. No space for chain coiling of soft segments is available due to the lack of chain-folding. Thus soft segments have to be oriented and more or less elongated in the vicinity of domain boundaries. Soft segments in styrene–butadiene as well as in ether–ester elastomers, however, may be randomly coiled without any restriction in the direct vicinity of the domains.

The diffuse nature of the phase boundary is detectable by means of small-angle X-ray scattering. The small-angle scattering intensity of irregular, globular, two-phase structures with sharp phase boundaries obeys Porod's law, which states that the intensity $i(\theta)$ drops asymptotically with the fourth power of the scattering angle, θ, except for a constant background i_0:

$$i(\theta) \simeq \frac{1}{\theta^4} + i_0 \tag{4}$$

Diffuse phase boundaries result in an additional damping factor $d(\theta)$, i.e. in a modified law:

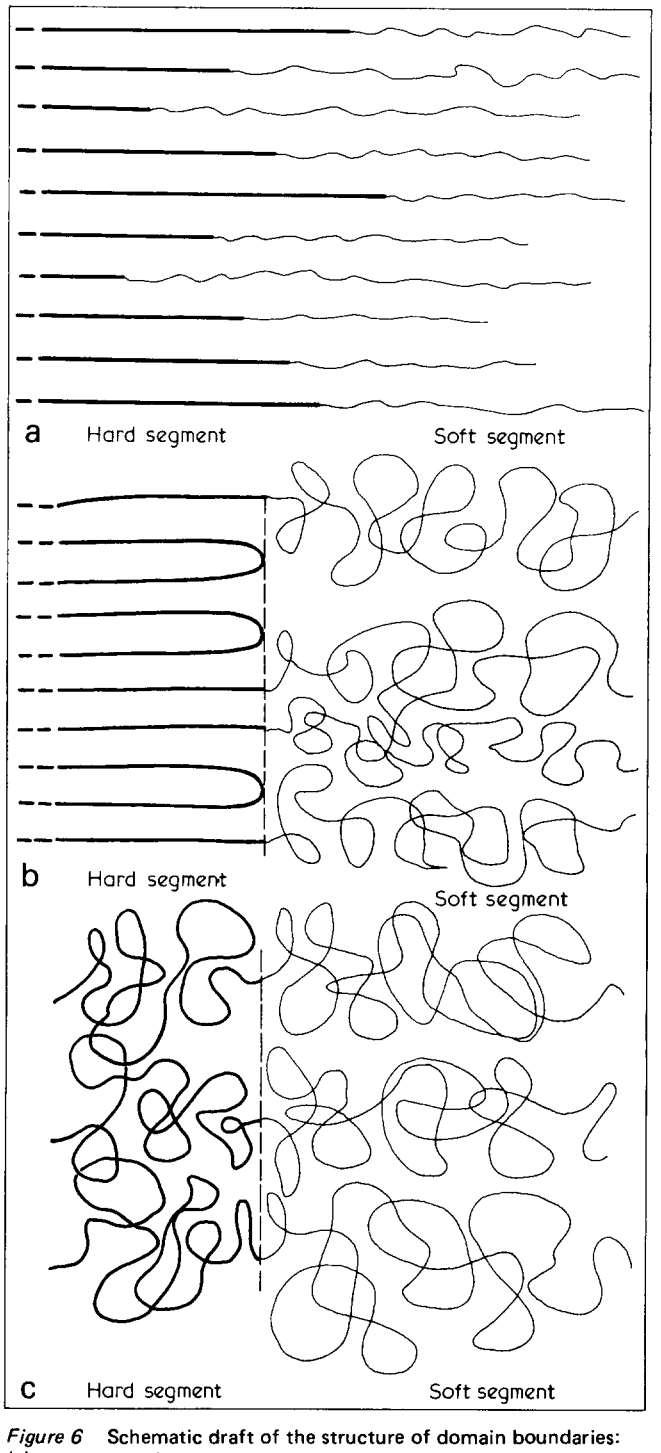

Figure 6 Schematic draft of the structure of domain boundaries: (a) in the case of segmented polyurethanes where no chain folding occurs; (b) in the case of crystallizable hard segments with chain-folding; (c) in the case of purely amorphous hard segment domains. No sharp domain boundaries are found in (a) contrary to (b) and (c). Due to the lack of hard segment chain-folding in (a), the soft segments close to the domain boundary are forced to be virtually elongated, whereas they may be randomly coiled in (b) and (c)

$$i(\theta) = \sim \frac{d(\theta)}{\theta^4} + i_0 \qquad (5)$$

Thus, information about the diffuse qualities of the phase boundary may be obtained from the experimentally determined damping factor. Inference on misordered hard segments dispersed in the matrix as well as soft segments running through the domains are simultaneously derivable from the small-angle scattering intensity.

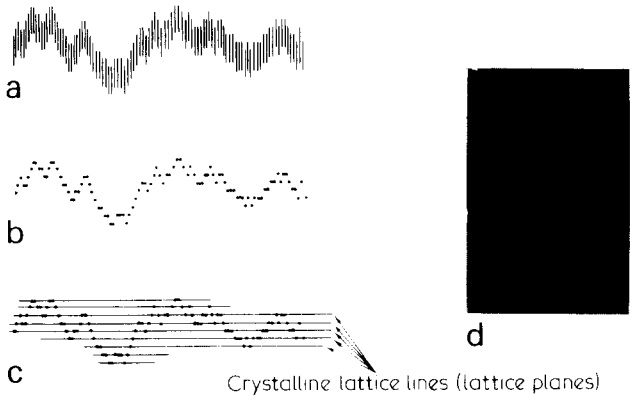

Figure 7 Optical Fraunhofer diffraction pattern of a model structure illustrating a structure proposition for the mutual arrangement of polyurethane hard segments within the domains. Although no vertical periodicity is found at any point in the structure, it still gives rise to meridional reflections due to the fact that the projection of the structure onto a vertical line is periodic

Diamine-extended segmented polyurethanes are commonly prepared with a ratio w of macrodiol to MDI (see equation 1) of about 0.5. Thus, the hard segments, each comprising on average $\bar{p} = 2$ or $\bar{p}' = 3$ MDI blocks, show no internal periodicity. Hence no crystallization can be expected in the conventional sense. Distinct reflections, however, are observable in the wide angle X-ray pattern showing a well-developed spatial coherence between neighbouring hard segments. In the case of a highly oriented hydrazine-extended material, these reflections are found on the meridion of the diagram indicating the existence of lattice planes perpendicular to the chain direction. This is hardly understood in terms of a conventional interpretation, since no suitable periodicity is found within the hard segments, as has already been mentioned. It was proposed, therefore, that these lattice planes be attributed to a well-defined longitudinal shift between laterally packed segments without referring to a longitudinal segment structure. This proposition is illustrated by the optical diffraction pattern in *Figure 7*, the structure being composed of dots which refer to the centres of gravity of laterally closely-packed hard segments pointing in the vertical direction. Although no longitudinal periodicity is found at any point in the structure, it still gives rise to meridional reflections due to the fact that the projection of the structure onto a vertical line is periodic. The interference diagram is consistent with the theory of paracrystals. Applying this theory it may be evaluated in all details.

In terms of the real structure, this proposition is examplified by *Figures 8* and *9*, which relate to hydrazine and

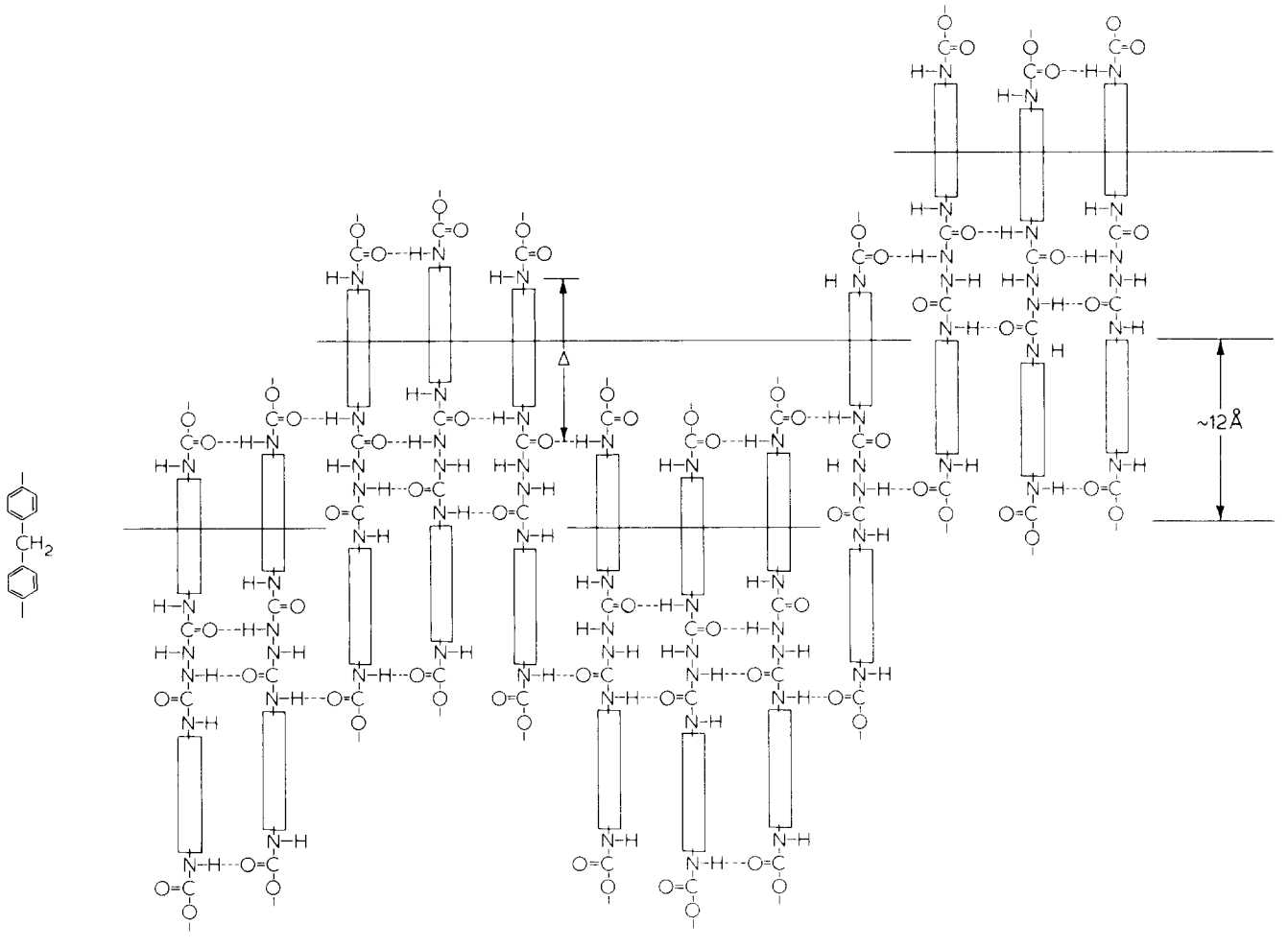

Figure 8 Schematic draft of the mutual arrangement of hydrazine-elongated polyurethane hard segments within a practically planar aggregate

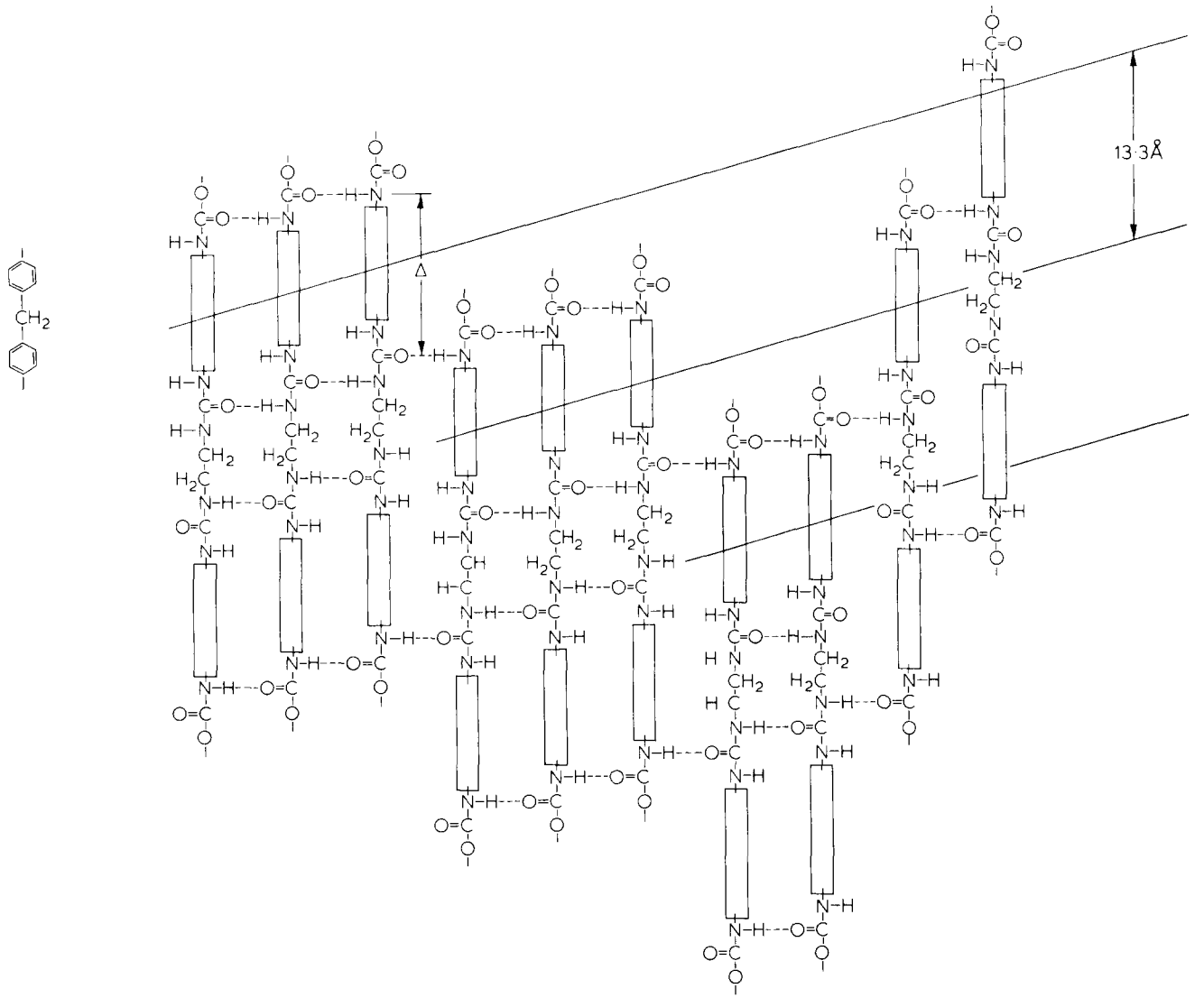

Figure 9 Schematic draft of the mutual arrangement of ethylene diamine elongated polyurethane hard segments

ethylene diamine, respectively, as chain extenders. Some of the neighbouring hard segments are packed laterally in a regular fashion, such that the urea groups are able to produce hydrogen bonds, while others are longitudinally shifted with respect to one another by an amount which is defined by the distance between urethane and urea groups. Although no conventional crystallization is brought about, singular lattice planes are found which lie orthogonally to the chain direction in *Figure 8* but which are slightly inclined in *Figure 9*. These lattice planes produce the hard segment reflections seen in the wide-angle X-ray diagram.

SOFTENING BEHAVIOUR AND CROSSLINKING STABILITY

The softening behaviour of segmented block copolymers may be studied by measuring the temperature dependence of the complex modulus. This holds true especially for the softening of the matrix. *Figure 10* shows results for three diol-extended polyurethanes prepared from the same polyester soft segment but with an increasing proportion of hard segments due to an increasing hard segment length. The pure polyester crystallizes with a melting point at about 40°C, but it does not crystallize in the elastomer except in material which has been extended by about 150 to 200%. The crystallization induced by stretching vanishes reversibly when the material is unloaded.

The glass transition of the pure polyester is found at about −57°C but the softening of the elastomer matrix takes place at about −35°C. Both the elevated softening temperature of the polyester as well as the lack of crystallization in the undeformed material are due to disordered hard segments which are randomly dispersed in the matrix. The softening temperature of the matrix remains constant irrespective of an increasing concentration of hard segments, but the softening process is more and more spread out towards higher temperatures with increasing hard segment length. This can be attributed to the diffuse nature of the domain boundary which is more pronounced the longer the hard segments are, since with increasing length an increasing spread in the length distribution is found. The softening of the matrix clearly starts at a certain distance from the domain boundaries, intruding more and more into the boundary zone with increasing temperature (see *Figure 6*). However, no asymmetry in the softening process is observable in the corresponding d.s.c. diagram (see *Figure 11*). We are thus inclined to distinguish between rate processes based on energy barriers which are

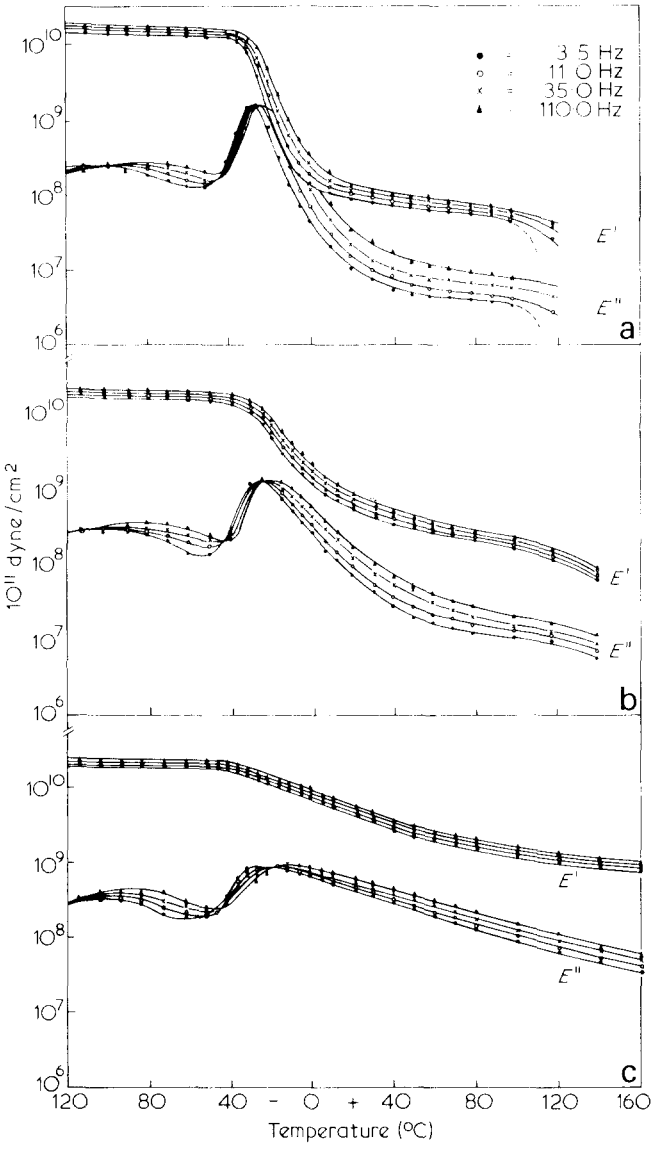

Figure 10 Temperature dependence of the complex modulus for butanediol-extended segmented polyurethanes with increasing volume fraction of hard segments, showing the softening behaviour of the matrix (after Hespe *et al.*)

temperature dependent and those which are temperature independent.

The d.s.c. signal of the glass transition indicates an increasing free volume which brings about an increase in volume energy. The corresponding lowering of energy barriers causes enhanced segment mobility. The mobility itself is not detectable from the d.s.c. diagram but the changing potential volume energy is. Thus, rate processes with temperature-independent energy barriers (since they are not associated with an increasing free volume producing an increase in potential volume energy) do not contribute to the d.s.c. signal. From the complex modulus (*Figure 10*) and the d.s.c. signal (*Figure 11*) it may be derived, therefore, that softening within the matrix starts with a free volume effect. Softening propagates into the boundary zone, however, without a free volume effect, this being prevented by the rigid arrangement of hard segments in this case. Softening of the boundary zone is clearly due to rate processes with temperature independent energy barriers.

Domain softening is indicated in the d.s.c. diagram in *Figure 11* by a number of discrete endothermic peaks. These could possibly be attributed to distinct domain sizes in the case where hard segments are fractionated according to their length. However, distinct domain sizes due to hard segment fractionation would imply sharp domain boundaries, whereas unsharp boundaries are indicated from the matrix softening behaviour (*Figure 10*).

Domain softening in diamine-extended polyurethanes does not correlate in general with any d.s.c. signal at all. This result is not yet properly understood. It is an open question whether domain softening in this case is entirely due to rate processes with temperature-independent barriers and hence without any free volume effect.

Domain softening has also been investigated by nuclear magnetic resonance, revealing proton mobility. Applying a suitable pulse technique, matrix protons may be distinguished from domain protons thus giving information about domain formation from the melt. It was found that domains of segmented polyurethanes become entirely dissolved in the matrix with increasing temperature. On cooling the melt it takes several hours before domains are reformed by diffusion processes which separate the hard and soft segments.

Softening measurements, although useful in general, do not allow direct determination of the crosslink spectrum as might be expected. Possible discrepancies between softening behaviour and crosslink spectrum become clear when comparing two different types of styrene–butadiene three block polymers, so-called SBS and BSB triblock copolymers. SBS-

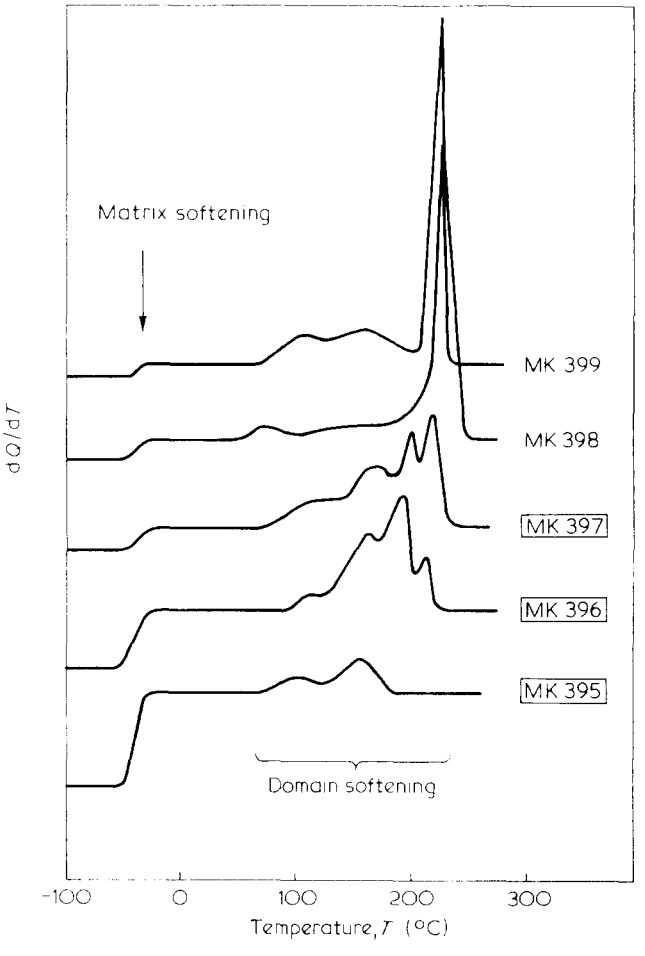

Figure 11 D.t.a. diagram of butanediol-extended segmented polyurethanes with increasing volume fraction of hard segments concerning the same samples as in *Figure 10*. The matrix softening shows no asymmetry (after Hespe *et al.*)

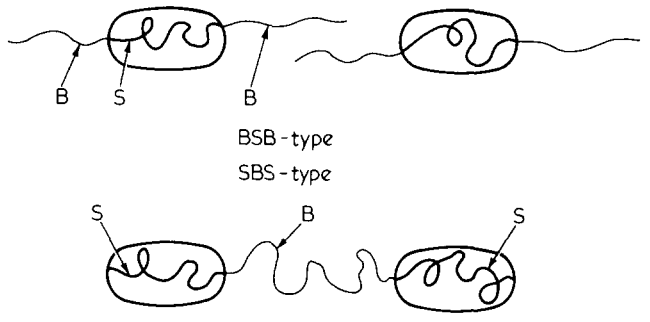

Figure 12 Schematic draft of the crosslink structure in BSB-type and SBS-type three-block copolymers

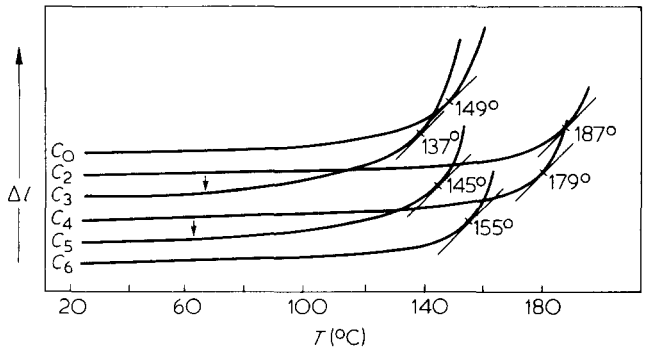

Figure 13 Temperature–extension curves for segmented polyurethanes with $H_2N-(CH_2)_n-NH_2 = C_n$ extenders for determining the heat-distortion temperature T_{HD}. It is systematically higher with n being even than with n odd

type chains provide one butadiene sequence, each of which is linked at both ends to styrene sequences. In the reverse BSB-type, chains are built up by two butadiene sequences with a styrene sequence between them. Apart from occasional chain-folding, SBS-type chains run from one domain to another, their styrene segments being embedded in two different domains such that two domains per molecule are involved (*Figure 12*). Thus, main valence interactions between the domains are brought about, and these cause load transmission from domain to domain on loading the material. An entirely different situation is found in the case of BSB-type chains. These are embedded in only one domain. Therefore, no main valence interaction is available in this case for load transmission between domains. Crosslinking breaks down in BSB-type material as soon as soft segment mobility sets in, i.e. when the softening temperature of the matrix is exceeded. In SBS-type material on the other hand crosslinking remains stable until hard segment mobility occurs when the softening temperature of the hard segment domains is exceeded. Nevertheless, one and the same d.t.a. diagram is found in both cases, provided that the ratio of styrene to butadiene and the same state of segregation is realized. This is similarly true for the temperature dependence of the complex modulus, which refers only to small segment rearrangements within the matrix, irrespective of whether or not main valence chains are present providing interaction between the domains. Softening measurements should therefore be obtained from creep experiments, which reveal main valence entanglements sustaining sufficient crosslinking stability between the domains.

Creep measurements are most easily performed by plotting the length of a sample heated continuously under constant load (see *Figures 13* and *14*). The length of the sample remains approximately constant within a certain temperature range and then shows a steep increase as soon as crosslinking starts to break down, thus defining the so-called heat distortion temperature T_{HD}. Temperature–extension curves of this sort provide preliminary information about the crosslinking stability which is useful for comparing different substances under the same conditions. However, the compliance instead of the length should be used for more accurate measurements, especially in those which are load-dependent. Furthermore, it is necessary to perform isothermal creep experiments.

Simple temperature–extension curves are shown in *Figures 15* and *16* for segmented polyurethanes with various diamine extenders and various soft segments. In both cases a variation in T_{HD} is observed. Chain extenders C_n $H_2N-(CH_2)_n-NH_2$ with an even number n of CH_2 groups are more effective than those with an odd number of CH_2 groups. T_{HD} is higher in the first case than in the second, even though the number of interacting urethane and urea groups is the same. The degree of cooperation between these groups, however, is different, as can easily be deduced from *Figure 9*. Chain extenders C_n with an even number of CH_2 groups provide a centre of symmetry which is absent in chain extenders with an odd number of CH_2 groups. This results in a maximum of four stress-free hydrogen bonds per MDI block in the first case but a maximum of only three in the second case.

It has been suggested that urea groups are able to contribute to hydrogen bonding in two different directions simultaneously, since each C=O group is balanced by two NH groups in the urea configuration. Two-dimensional crosslinking systems, as shown in *Figures 8* and *9*, require only one NH group per C=O group, such that a certain proportion of the NH groups does not take part in the system. It is reasonable to assume, however, that additional hydrogen bonds are formed perpendicular to the plane of the diagram in *Figures 8* and *9*. These bonds are maintained by the extra NH groups. Two-dimensional crosslinking systems are enlarged in this way into three-dimensional systems. This is in accordance with the results of wide-angle X-ray diffraction measurements.

The assumption that transverse crosslinking is necessary for satisfactory crosslinking stability leads to an interesting understanding of some of the characteristics of diol extension. Butanediol-extended polyurethanes are commonly prepared with a molar ratio of macrodiol to MDI, w, of less than

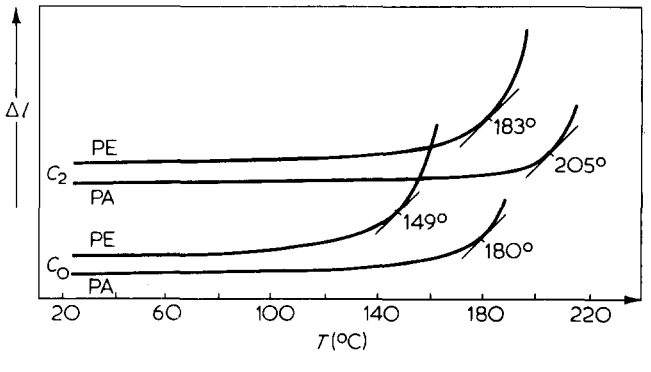

Figure 14 Temperature–extension curves for segmented polyurethanes with C_0 and C_2 extenders comprising an ether or ester soft segment, polyethylene and polyester, respectively

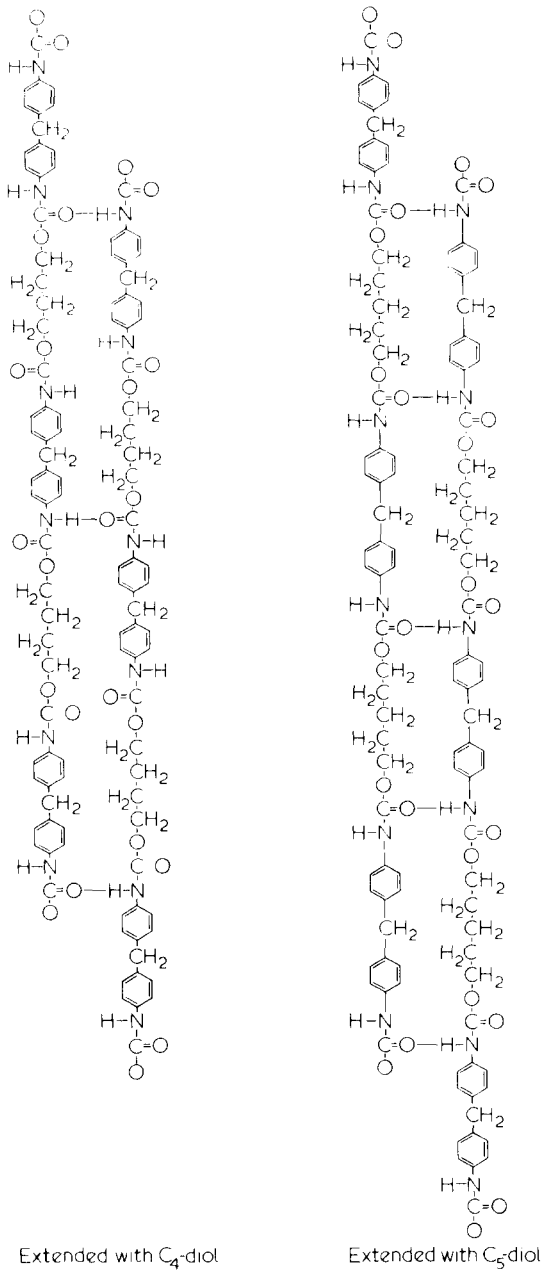

Figure 15 Steric conditions for forming hydrogen bonds between butanediol and pentanediol extended hard segments, respectively

approximately 0.3. More than 3 (i.e. $\bar{p} = 3$) or 4 ($\bar{p}' = 4$) MDI blocks are thus found on average in each of the hard segments, $\bar{p} = 3$ or $\bar{p}' = 4$ being the minimum number necessary to obtain a material with elastomeric properties. In diamine-extended materials the minimum occurs with $\bar{p} = 2$ or $\bar{p}' = 3$. This is probably not due solely to the stronger interaction of urea compared with urethane groups, but is a consequence of the fact that urethane groups may contribute to hydrogen bonding in one direction only, whereas urea groups are effective in two different directions simultaneously. Transverse crosslinking in diol-extended materials is brought about only by some of the urethane groups being effective in one direction while others are effective in a transverse direction, with the result that a greater number of interacting groups per hard segment is required than in diamine-extended hard segments. This conclusion has been verified recently by crystallographic investigations performed on low molecular weight model compounds.

The importance of transverse crosslinking is also shown by pentanediol reducing the crosslinking stability when used as chain-extender instead of butane diol. Pentanediol-extended segments fit more easily together than butanediol-extended segments (see *Figure 15*) such that all urethane groups found in a segment are able to form hydrogen bonds within a two-dimensional planar aggregate of segments. However, the perfect planar cooperation between neighbouring segments prevents transverse crosslinking, since no urethane groups supporting transverse crosslinking are available. Crosslinking stability, which may be characterised by the heat distortion temperature T_{HD} at which domain softening occurs, depends on the chemical nature of the chain extender, the hard segment length and the domain size. It is further controlled by the microstresses on the domains caused when the material is loaded externally. Stress concentrations arise, which are influenced by the volume fraction, shape, size and spatial arrangement of the domains. Additional molecular stress concentrations have to be taken into account, due to the varying lengths and the individual situations of different soft segments.

Crosslinking stability, defined by the stability of the hard segment domains, also depends on the nature of the soft segments even though they do not contribute directly to the domains. Domain formation, however, implies the segregation of hard and soft segments which show a certain mutual solubility. The greater the mutual solubility, the poorer the segregation, resulting in an increasing microstress on the domains with decreasing volume fraction. T_{HD} drops, therefore, when the mutual solubility of hard and soft segments is

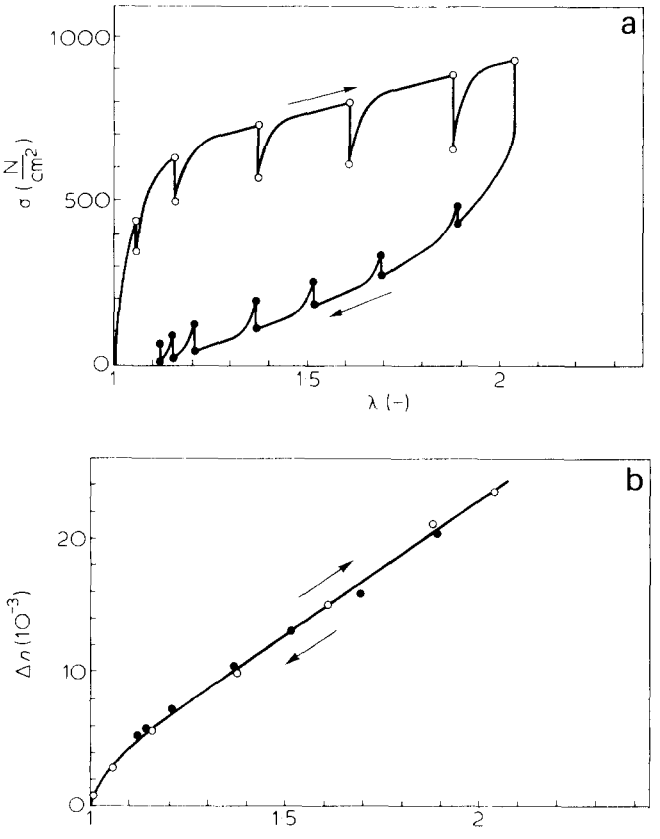

Figure 16 Strain birefringence of diol-extended segmented polyurethanes: (a) stress–strain behaviour of a sample which was stepwise elongated and subsequently stepwise released. In spite of relaxations and in spite of hysteresis between loading and unloading, neither relaxation nor hysteresis is seen in the birefringence (b)

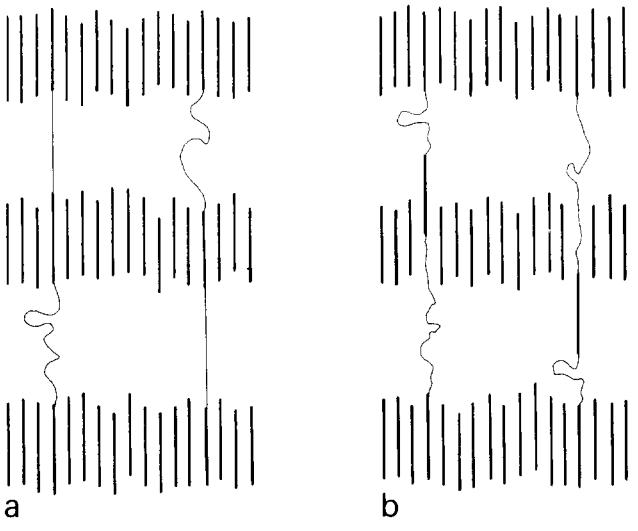

Figure 17 *Ad hoc* explanation for the result shown in *Figure 16* assuming that relaxation and hysteresis are due to an increasing homogeneity of the spatial distribution of local stresses and molecular orientation, whereas the average molecular orientation remains constant

increased. This is the case for an ester soft segment in comparison with an ether soft segment, since the ester affinity for urethane segments is greater than the ether affinity (see *Figure 14*). The actual situation is a little more sophisticated, as will be reported at a later date. Nevertheless, the overall results hold true, that ether soft segments give rise to a more complete segregation than ester soft segments. The heat distortion temperature is additionally lowered in this case due to a more inhomogeneous molecular load transmission caused by a broader molecular weight distribution of ester compared with ether soft segments. It has not yet been fully established whether the less complete segregation or the more inhomogeneous load transmission is the more important factor in lowering T_{HD}.

Crosslinking stability as determined from temperature-extension measurements is related simultaneously to both thermally- and mechanically-stimulated domain softening. However, thermal stimulation is considered to be predominant as long as the measurements are performed under constant load. These measurements must be supplemented, therefore, by load-dependent measurements in order to obtain a more complete picture of the crosslinking strength. No systematic work in this field is known at present.

Stress- or strain-induced domain softening is clearly domonstrated by stress–strain curves when the material is loaded and unloaded cyclically with increasing maximum load (*Figure 4*). Loading and unloading produce a remarkable hysteresis. Furthermore, a break is seen in the curve as soon as the maximum load of the previous cycle is exceeded. This break indicates plastic deformation of those domains which suffer a high local stress concentration either on a molecular scale produced by single soft segments or on a morphological scale produced by an irregular spatial arrangement of domains. The higher the local stress concentrations are initially, the more they are reduced, thus improving the homogeneity of internal load transmission. The break in the curve points to a specific crosslinking instability reducing the retractive force, but producing a more stable crosslinking situation. Unloading and subsequent reloading gives rise only to a rather small hysteresis. Unstable crosslinks are removed and simultaneously transformed into more stable crosslinks. They are not simply broken down, since in this case the stress reached in the previous cycle could not be reached again in the following cycle. The crosslinking is remodelled by domain deformation. This also applies to the heat distortion temperature which increases as a result of previous deformation. Thus the results obtained are varied, depending on pretreatment, such that no systematic understanding of the structure – property relationship can be gained from them. We shall return to this problem in the following section.

The variation in load transmission due to domain deformation is correlated with another somewhat puzzling effect, shown in *Figure 16*, which refers to (a) the stress–strain behaviour and (b) the stress birefringence of a diol-extended polyurethane. Virtually the same results are obtained with any other segmented polyurethane. Whether this is also true for other segmented block copolymers is not yet known.

The sample under investigation was extended in a stepwise manner. After each step it was held at constant length for a period of time so that relaxation could take place. The birefringence was measured at each step in the relaxed state. This was performed during loading as well as unloading, i.e. with increasing and decreasing load. Although the stress was very different on the loading and unloading paths, no difference in stress birefringence was observable when referring to the same strain, i.e. stress birefringence was dependent only on strain. Relaxation takes place without any loss in molecular orientation. A schematic *ad hoc* explanation is shown in *Figure 17*, where it is assumed that relaxation is due to the breaking of secondary valence interactions between neighbouring hard segments in such a way that the overall orientation of segments remains unaffected. The spatial distribution of orientation becomes more uniform during relaxation; hence, in addition to the orientation entropy for Gaussian networks, a spatial orientation distribution entropy has to be taken into account. This may increase during relaxation without any change in orientation entropy.

Both wide-angle X-ray measurements and dichroic infrared measurements have shown that hard segments become systematically disoriented transverse to the extension direction up to an elongation of about 150 to 200%. At higher elongations hard and soft segments become aligned parallel to the extension direction. In the region of about 150 to 200% elongation, relaxation takes place in such a way that hard segment orientation increases whereas soft segment orientation decreases. These processes partly compensate each other. Inhomogeneous load transmission to the domains gives rise to a torque (see *Figure 17*) which is reduced by domain deformation.

FREEZING-IN AND SOFTENING OF ELEMENTARY STRESSES AND STRAINS

Crosslinking in thermoplastic elastomers may be described by the number of crosslinks per unit volume $N(T,t,f,\ldots)$ in a corresponding Gaussian network which would show, under the same conditions, the same retractive force f as the sample under investigation. The crosslinking density defined in this way depends on temperature T, time t, load f, extension ratio $\lambda = 1 + \epsilon$ and thermomechanical history. Temperature and time dependence may be represented by a suitable set of Maxwell elements (see *Figure 1*), or, more conveniently with respect to creep measurements, by a corresponding system of Kelvin–Voigt elements (*Figure 18*). Both Maxwell and Kelvin–Voigt systems are well known from the analysis of linear viscoelastic effects. They are also useful for charac-

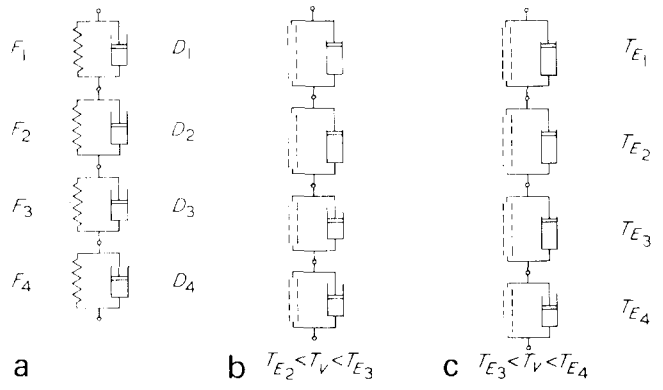

Figure 18 Kelvin–Voigt representation of the crosslink spectrum. This is more convenient for creep experiments than the Maxwell representation (*Figure 1*)

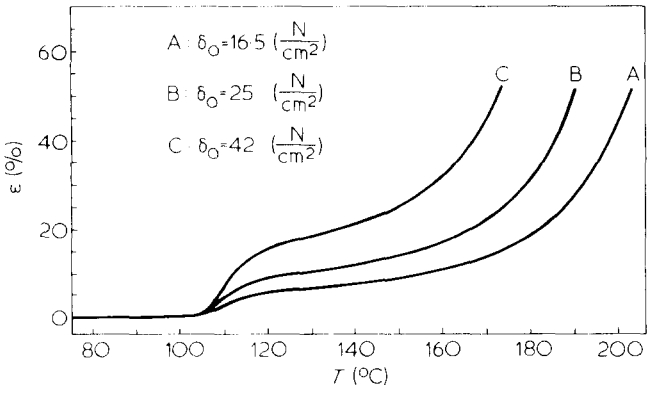

Figure 19 Temperature–extension curves for high molecular weight PMMA showing the glass transition at about 105°C and the flow transition above 170°C

terizing the crosslink spectrum of thermoplastic elastomers. This will be illustrated in the following example, referring for simplicity to high molecular weight PMMA instead of a segmented block copolymer. The phenomenological results are much the same in both cases, although the structural parameters are different.

The PMMA which was investigated has a molecular weight of about 10^7. It is fully atactic and thus completely amorphous, so that no morphological changes have to be taken into account. Due to its high molecular weight, a large number of chain entanglements are present; these cause rubber elasticity above T_g. Only a negligible amount of viscous flow is superimposed onto this. The effective number of chain entanglements is only temperature- and time-dependent, thus representing a very simple crosslink spectrum as the model for the more complex situation found with segmented block copolymers.

The temperature–strain curves of *Figure 19* show a glass transition at ~105°C and a flow transition above 170°C. Rubber elasticity is found from 120° up to about 170°C or even higher depending on the loading time. The compliance is approximately independent of load, strain and history.

A more detailed picture of the crosslink spectrum can be obtained from isothermal creep measurements. *Figure 20* shows a set of creep results for PMMA at a single applied stress. (Dependence of the creep behaviour on applied stress will not be discussed here.) The amount of viscous flow occurring at each temperature can be determined from the straight part of the creep curve (i.e. at long times when viscoelastic deformation has ceased) and by extrapolating back to $t = 0$. Viscous flow is seen to be negligible up to approximately 140° C. At 180°C a viscous flow of approximately 4% is found after a loading time of 300 s and 11% after 900 s, compared with a viscoelastic elongation of about 22% in both cases. Since viscous flow does not give rise to any retractive force, it has to be subtracted from the overall elongation when discussing the crosslink spectrum. A time-independent viscoelastic elongation (after subtraction of viscous flow) is reached in 30 to 200 s after the load is applied. This equilibrium strain ϵ_∞ is sensitively dependent on temperature and corresponds to a temperature-dependent partial instability of the crosslinking. The isothermal viscoelastic elongation of a Kelvin–Voigt system comprising n elements is described by:

$$\epsilon(t) = \sum_{i=1}^{n} \epsilon_i(t) = f \sum_{i=1}^{n} \{1 \quad C_i e^{-\beta_i t}\} \rightarrow \epsilon_\infty(T)$$

where f is the applied load, C_i are the compliances and β_i the creep rates of the n elements.

$$\epsilon_i(t) = f\{1 \quad C_i e^{-\beta_i t}\}$$

will be called an elementary strain, being related to the elementary stress $f_i(t)$ by:

$$f_i(t) = \frac{\epsilon_i(t)}{f}$$

The creep rates in *Figure 20* do not increase steadily with temperature but do so discontinuously at distinct temperatures. This can be seen clearly from the creep curves at 120° and 140°C. In terms of Kelvin–Voigt elements, some are highly mobile in this temperature range, while others are rigid, but no elements are found showing moderate mobility. The ratio of mobile to rigid elements is sensitively dependent on temperature. Elements which are rigid at T_1 are highly mobile at T_2 only one or two degrees above T_1. The situation is different in the glass transition region as well as in the flow transition region, where a more steady increase in the creep rates is observed.

Each Kelvin–Voigt element represents a partial crosslink-

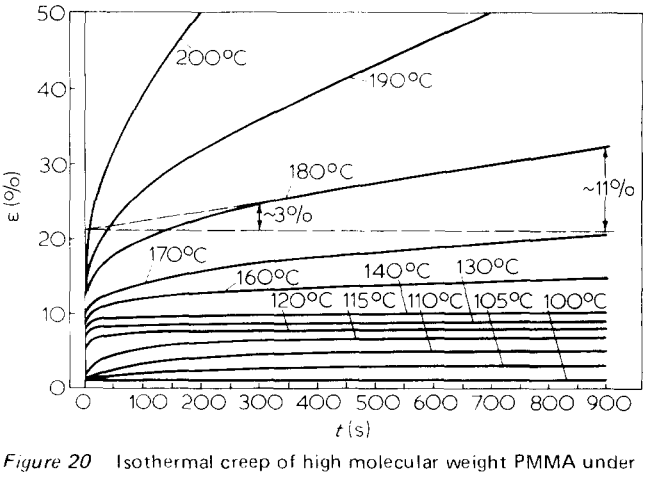

Figure 20 Isothermal creep of high molecular weight PMMA under constant load

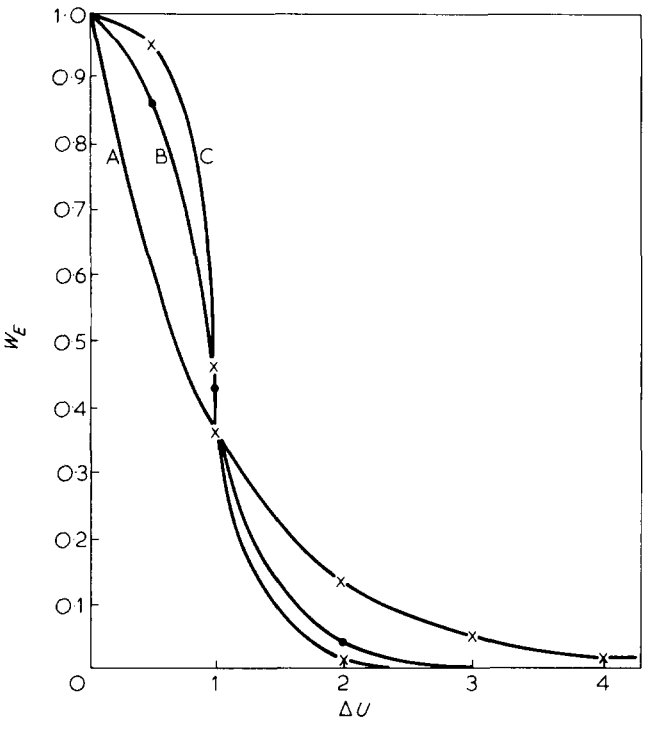

Figure 21 Activation probability for overcoming an energy barrier with (a) one, (b) two and (c) three vibrations involved (after Holzmüller)

ing which is stable up to a particular temperature but which breaks down within a narrow temperature range of only a few degrees. Thus the overall softening of the material is brought about by superimposed elementary softening processes each related to a partial crosslinking. Considering the softening of a partial crosslinking to be due to a rate process, we could be tempted to calculate the activation energy controlling the crosslinking stability from the derivative $\delta\epsilon_\infty/\delta T$ with the aid of the Arrhenius equation. This would be misleading, however, since cooperative molecular vibrations are involved.

The Boltzmann energy distribution can be written as:

$$\omega_E = \exp(-E/kT)/Z$$

where Z is the partition function. In the case of a one-dimensional harmonic vibration, Z is given by $Z = kT$ resulting in an energy distribution:

$$\omega_E = \exp(-E/kT)/kT$$

The activation probability

$$\omega_A = \sum_{\Delta E}^{\infty} \omega_E \mathrm{d}E = \mathrm{e}^{-E/kT}$$

is found from this energy distribution by integration, the energy barrier being taken as the lower limit. From this calculated activation probability the activation energy may be evaluated with the aid of an Arrhenius plot. This procedure, however, is based on the assumption that only one vibration is involved, corresponding to a second order reaction. The real process is characterized by a large number of vibrations, giving rise to an energy barrier the height of which is randomly fluctuating. In the case where all vibrations involved in overcoming the energy barrier share their whole energy, the activation probability of the ensemble will be given by:

$$\omega_A = \mathrm{e}^{-\Delta E/kT}\left\{1 + \frac{\Delta E}{kT} + \frac{1}{2!}\left(\frac{\Delta E}{kT}\right)^2 + \frac{1}{3!}\left(\frac{\Delta E}{kT}\right)^3 + \ldots + \frac{1}{(s-1)!}\left(\frac{\Delta E}{kT}\right)^{s-1}\right\}$$

where s is the number of cooperating vibrations. Taking into account share ratios between zero and one in order to characterize the influence of each vibration on the rate process, more complicated results will be found depending on the number of vibrations and their share ratios. These will not be discussed in detail here. As a general rule, however, it turns out that the activation probability drops much faster at about $kT = \Delta E$ than with only one vibration, as seen from *Figure 21*. This leads to a value for the activation energy from the Arrhenius equation which is far too high. The activation probability based on cooperating vibrations shows more or less a 'yes–no' character, indicating that practically all systems are activated at $kT \gtrsim \Delta E$, whereas practically no system is able to overcome the barrier at $kT \lesssim \Delta E$. This theoretical result corresponds very well with the experimental findings in *Figure 20*. Consequently, we are dealing with either mobile or rigid elements with practically nothing in between, without being forced to adopt an activation energy whose value would be unbelievably high.

STRESS AND STRAIN CROSSLINKING

On deforming a sample at a given temperature, elements which are mobile will be strained while other elements which are rigid remain unaffected. Thus we obtain a distribution of elementary stresses and strains which depends on temperature, strain and loading time. As the deformed sample cools, one strained element after another freezes-in, due to crosslinks becoming effective which were not effective at the straining temperature. This illustrates the fact that two different aspects of crosslinking have to be considered: a conventional crosslinking relating to the retractive force of a deformed sample and an additional crosslinking stabilizing the deformation. The conventional aspect refers to the so-called 'stress' system of crosslinking. This is formed in the undeformed state of the material and is what produces the stress when the material is loaded. The additional aspect refers to the so-called 'strain' system of crosslinking, which is created when the material is in a strained or deformed state. The strain crosslinking stabilizes the deformation, i.e. 'produces' strain. Stress crosslinking is predominant at the deformation temperature, virtually no strain crosslinking being present at all. The stress crosslinking becomes weaker on heating the deformed material, due to overall crosslinking instability, without the formation of any strain crosslinking. However, it remains stable on cooling the deformed material, becoming more and more balanced by strain crosslinking which develops with decreasing temperature. Strain crosslinking is predominant in the frozen-in state, i.e. it prevents the stress crosslinking from becoming dominant by inhibiting a macroscopic retractive force.

Strain crosslinking is formed from interactions which are not effective at the deformation temperature but which be-

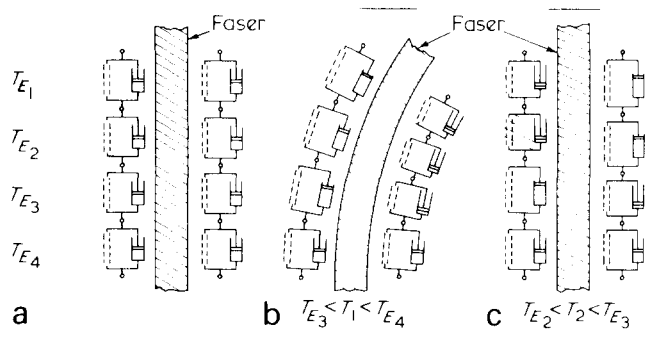

Figure 22 Texturing of synthetic fibres as an example for stress and strain crosslinking producing memory effects

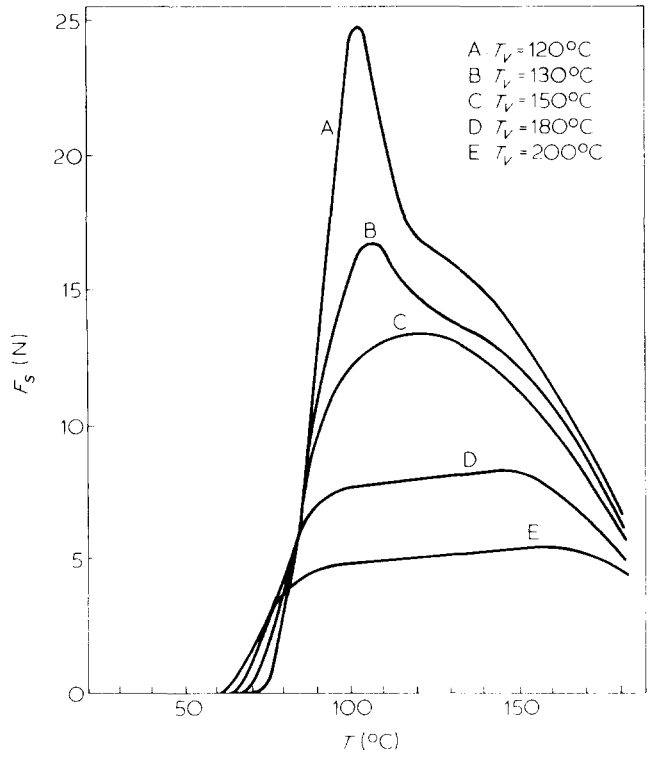

Figure 23 Shrinkage force of PMMA samples elongated by 100% at different temperatures. The elongated samples were frozen-in by quenching, and were subsequently reheated

come effective on cooling the specimen. Stress crosslinking, however, is based on interactions which are stable at the deformation temperature. On heating a deformed, frozen-in sample the initially predominant strain crosslinking breaks down successively, whereas the stress crosslinking remains unaffected and becomes free to produce macroscopically observable stress. Since stress and strain crosslinking are based on one and the same crosslink spectrum, the same softening temperatures of the partial crosslinking apply to both. The crosslink spectrum is reflected, therefore, in both creep and shrinkage measurements.

When a material undergoes a complicated thermomechanical history, more than one stress and one strain crosslinking system have to be considered. Producing such systems is a widely used technqiue to improve the properties of, for example, Spandex or Elastan fibres, as well as to produce special effects with polyamide or polyacrylonitrile fibres. This can be summarized under the term 'thermosetting'. We refer for illustration to the well-known texturing of fibres in a simplified manner as follows. Let us consider a sample being bent in one direction and subsequently re-bent such that it becomes straightened out again (*Figure 22*). Bending and re-bending are performed at different temperatures T_1 and T_2, respectively, thus giving rise to stress and strain systems as indicated in *Figure 22* by the four Kelvin–Voigt elements on each side of the sample. If bending takes place at a temperature T_1 in between T_{E3} and T_{E4} three elements on each side become extended or compressed, respectively. On cooling the deformed sample to a temperature T_2 in between T_{E2} and T_{E3} the element '3' freezes-in in the deformed state due to a partial strain crosslinking being created. On re-straightening the specimen, the frozen-in elementary strain in '3' remains unaffected but it has to be compensated by opposite deformations of the elements '2' and '1'. On cooling the restraightened sample below T_{E1}, all elementary deformations become stabilized by corresponding partial strain crosslinking forming a suitable strain system. These systems give rise to a memory effect, since on reheating the frozen-in sample a spontaneous bending will initially be produced followed by a spontaneous straightenening at higher temperatures.

These model considerations will be examplified in the following by shrinkage measurements on high molecular weight PMMA, which was strained by 100% at different temperatures and subsequently quenched in ice water. Straining and quenching were performed in 10 s. The higher the deformation temperature, the greater the number of elements experiencing the same elementary stress, directly applied by the external load. The elements are strained differently, however, according to their respective compliances. Elements which are rigid at the deformation temperature remain unaffected. On reheating a frozen-in sample at fixed length, strain crosslinks formed during quenching break down, enabling stress crosslinking to produce an external shrinkage force (*Figure 23*). In order to avoid buckling due to thermal expansion of the frozen-in sample, measurement of the shrinkage force starts with a prestress which drops with increasing temperature. Under suitable conditions the retractive force reaches zero when the shrinkage force starts to develop. This is seen in *Figure 25*, but the initial part of the measuring curves is omitted in *Figure 23* for simplicity. Whether or not the retractive force actually reaches zero when shrinkage forces set in has no bearing on the results. Shrinkage forces start to develop between 60° and 70°C. For a sample extended at 200°C, the shrinkage force shows an approximately constant value from about 90° to 170°C except for a slight increase which reveals its entropic nature. On extrapolating

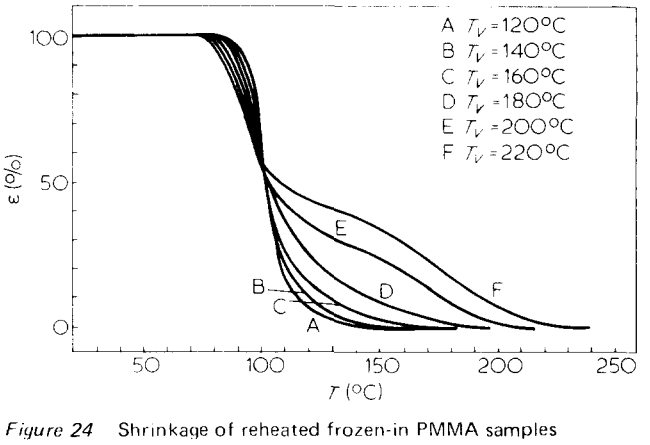

Figure 24 Shrinkage of reheated frozen-in PMMA samples

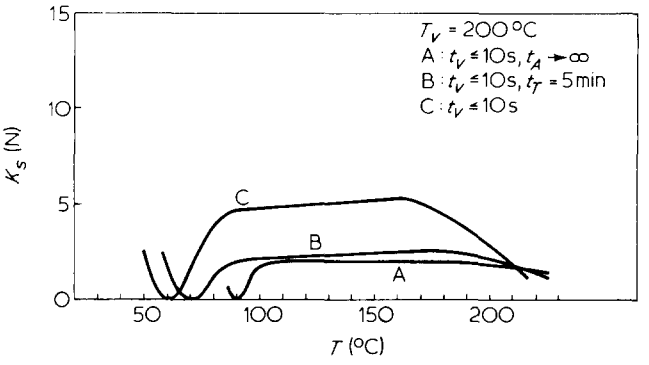

Figure 25 Shrinkage force of reheated PMMA samples which were frozen-in under different conditions

the shrinkage force to lower temperatures, the results would pass through absolute zero (*Figure 23*).

Elements with a softening temperature up to about 170°C clearly experience the same elementary stress. However, elements with softening temperatures above 170°C are not completely loaded in spite of the deformation temperature of 200°C. This occurs because the deformation time of only 10 s was too short compared with the retardation time of the elements which become soft just below the deformation temperature, allowing them to become completely loaded. These elements start to yield, therefore, under the stress of the less stable but more completely loaded elements. This gives rise to stress relaxation, i.e. to the shrinkage force dropping above 170°C.

Figure 23a refers to a sample which was deformed at 120°C, such that the whole elongation is stored in only a few rather unstable elements, which consequently become highly strained and experience high elementary stresses. A steeply increasing shrinkage force is found, therefore, which drops with approximately the same slope as soon as incompletely strained elements become mobile. From the position of the maximum it is seen that only elements with a softening temperature slightly below the deformation temperature have become incompletely loaded. This occurs because their retardation times are too long compared with the straining time. This is the same as the effect mentioned previously with respect to *Figure 23e*.

The decrease in shrinkage force with increasing temperature is due to a reorganization of elementary stresses. This takes place as soon as elements become mobile; because they are less loaded, these start to yield under the stress of the more unstable elements. This occurs without any loss of the stored deformation. *Figures 23a* and *23b* show a break occurring at about 120° and 150°C, respectively, which is related to corresponding breaks in *Figure 19* indicating a decrease or increase, respectively, in the elementary compliances.

On reheating a frozen-in sample with free ends, the elementary strains seen in *Figure 24* become observable. *Figure 24a* refers to a sample extended at 120°C, such that the whole deformation is stored in elements with softening temperatures below or up to 120°C. The sample retracts to its original length in only one step, which takes place when the straining temperature is reached again. At a deformation temperature of 220°C (*Figure 24f*) the stored deformation is distributed over elements with softening temperatures up to 220°C. The original length of the sample is reached only step by step in this case. Shrinkage commences at about 70°C and continues until 220°C, since some strained elements which are frozen-in at 200°C will become mobile, for example, at 210°C. The shape of the curve is roughly the same as in *Figure 19a* except for the fact that flow in *Figure 19* rises (in principle) to infinity whereas shrinkage in *Figure 24* comes to an end when the original length of the sample is reached.

So far we have discussed stress and strain crosslinking based on an invariant crosslink spectrum. This is in contradiction to the fact that shrinkage (see *Figure 24*) sets in at about 60° to 70°C, whereas creep (see *Figure 19*) does not develop below 105°C. The discrepancy cannot be explained by elementary stresses coming into action which are larger than the external load in the creep experiment, because the temperature of initial shrinkage falls with decreasing elementary stress. This is clear in *Figure 23* as well as in *Figure 24*. However, the discrepancy can be attributed to a variation in the crosslink spectrum because of the free volume which becomes frozen-in when the sample is quenched. From density measurements, it can be seen that the free volume will increase with increasing deformation temperature, resulting in a decrease in crosslinking stability. This is in accordance with the fact that the initial shrinkage takes place at a temperature which is lower, the higher the initial deformation temperature was. The free volume effect can further be illustrated by a variation in the cooling conditions.

Figures 25 and *26* show the shrinkage and shrinkage force, respectively, for three samples which were extended at 200°C: (a) cooled slowly at constant length; (b) held at the deformation temperature for 5 min and subsequently quenched in ice water; and (c) being quenched immediately after extension. Shrinkage sets in for case (a) at 105°C, sufficiently in accordance with T_g seen from *Figure 19*. Initial shrinkage takes place in cases (b) and (c) well below T_g at approximately the same temperature, since in both cases the same free volume is frozen-in.

The shape of the three curves is different as a result of an internal reorganization of elementary stresses and strains. The overall deformation becomes stored in more stable elements when the sample is held for a certain time at elevated temperature. This also includes elements whose softening temperature is higher than the deformation temperature. *Figure 26* is correspondingly understood, since the larger the number of elements to become strained the smaller the elementary stresses will be, provided that the overall deformation remains constant.

This refers once more to a relaxation process which takes

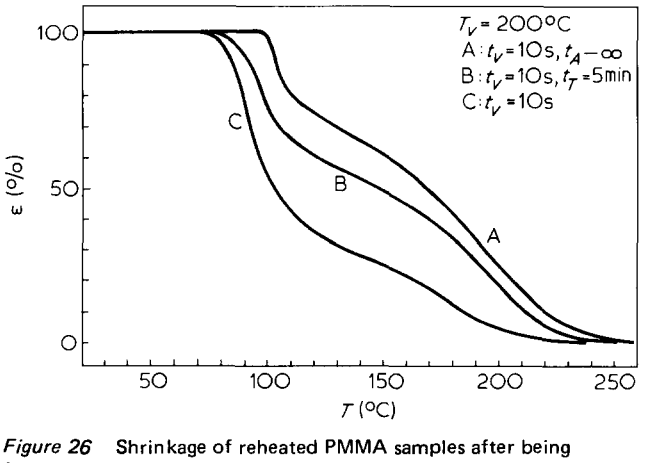

Figure 26 Shrinkage of reheated PMMA samples after being frozen-in under different conditions

place without any loss of the stored deformation.

The measurements in *Figures 25* and *26* reveal different distributions of elementary stresses and strains, based on one and the same crosslink spectrum in cases (b) and (c) but on a slightly modified spectrum in case (a) due to different cooling conditions. Similar variations of the crosslink spectrum are brought about in segmented block-copolymers by stretch-induced crystallization which sometimes gives rise to a somewhat confusing situation. We feel sure that an anlysis of the phenomenological results will be promoted by distinguishing the distribution of elementary stresses and strains from the crosslink spectrum of the material.